FELLOWSHIP FINAL REPORT

Molecular modeling of stretchable electronics

Yun Hee Jang,[a,b,c,d] Yves Lansac[a,b,c]

[a] Department of Energy Science and Engineering, DGIST, Daegu 42988, Korea
[b] GREMAN, CNRS UMR 7347, Université de Tours, 37200 Tours, France
[c] Laboratoire de Physique des Solides, CNRS UMR 8502, Université Paris-Saclay, 91405 Orsay, France
[d] Le Studium Loire Valley Institute for Advanced Studies, 45000 Orléans, France

REPORT INFO

ABSTRACT

A theoretical prediction of favorable ion exchange between PEDOT:PSS and hard-cation-soft-anion ionic liquids (IL) is confirmed experimentally and computationally by treating PEDOT:PSS with a new IL composed of an extremely hard protic cation MIM$^+$ and an extremely soft anion TCB$^-$. This protic IL significantly improves both conductivity and stretchability of PEDOT:PSS, outperforming its aprotic counterpart, EMIM :TCB, which has been the best IL employed for this purpose so far. This electrical and mechanical enhancement is speculated as a result of the aromatic and protic cation MIM$^+$ which does not only provide efficient ion exchange with PEDOT:PSS but also serves as a molecular glue holding together multiple PEDOT domains by strong ionic as well as hydrogen bonds, because washing MIM$^+$ out of the film degrades the stretchability while keeping the morphology. Our results offer molecular-level insights on the morphological, electrical, and mechanical properties of PEDOT:PSS and a molecular-interaction-based enhancement strategy for intrinsically stretchable conductive polymers.

1- Introduction

Materials constitute such an important aspect of civilization that our history is often defined by materials: the stone age, the bronze age, the iron age, and then the polymer-plastic age (Fig. 1). What about now? Since a germanium transistor was invented in 1948, we are surrounded by all kinds of electronic devices containing silicon semiconductors. No one would deny that we now live in the silicon age.

A conducting polymer with π conjugation along alternating single-double bonds of its backbone was discovered in 1977. The flexibility of such organic semiconductors or synthetic metals is a critical feature for realizing foldable phones and rollable TVs as well as artificial skin, artificial retina, and other biomedical implants. Organic soft (bio)electronics using them are slowly replacing or complementing silicon-based hard electronics. Wearable devices such as Apple Watch will soon be replaced by skin-like patch devices, which can even go inside our body to correct irregular heartbeats or improve our brain functions. We are now entering the renaissance of the polymer age (Fig. 1).
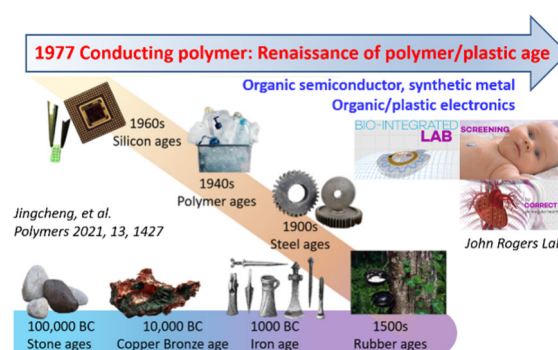

Figure 1. Materials and human history. With the advent of soft and stretchable skin-like electronics made of organic semiconductors, we enter the renaissance of polymer age.

A current key player in organic bioelectronics is PEDOT:PSS, a mixture of positively-charged poly-3,4-ethylenedioxythiophene PEDOT$^+$ and negatively-charged poly-styrenesulfonate PSS$^-$

Y. Jang, Y. Lansac. Molecular modeling of stretchable electronics, *LE STUDIUM Multidisciplinary Journal*, **2023**, *7*, 34 – 42

https://doi.org/10.34846/le-studium.255.01.fr.01-2023

34

(Fig. 2). This lightweight, flexible, stretchable, conformable, printable, wearable, transparent, skin-like, thermoelectric, and water-processable (mass-producible and environmentally-benign) ionic semiconductor/electrochemical transistor has been used to realize various flexible organic devices such as LED, solar cells, thermoelectric generators, self-powered implantable sensor-actuators, and ultimately artificial skins.

However, even such a state-of-the-art organic semiconductor shows a much lower electrical conductivity than its inorganic counterpart, ITO (indium tin oxide). The conductivities of vapor-deposited PEDOT crystals can be higher, but water-processed PEDOT:PSS films show very poor conductivities, because two types of ionic polymers of opposite charges and different lengths (PEDOT$^+$ of 6~18 EDOTs and PSS$^-$ of ~2000 SS units) are electrostatically bound to form granular domains. In each domain of 10-30 nm, a hydrophilic-but-insulating PSS-rich region surrounds a conducting-but-hydrophobic PEDOT-rich region (Fig. 2), making it water-soluble and stable, but hindered formation of conducting network of large PEDOT domains leads to a poor conductivity.[1-11] A tremendous amount of effort has been focused on enhancing the conductivity of PEDOT:PSS.
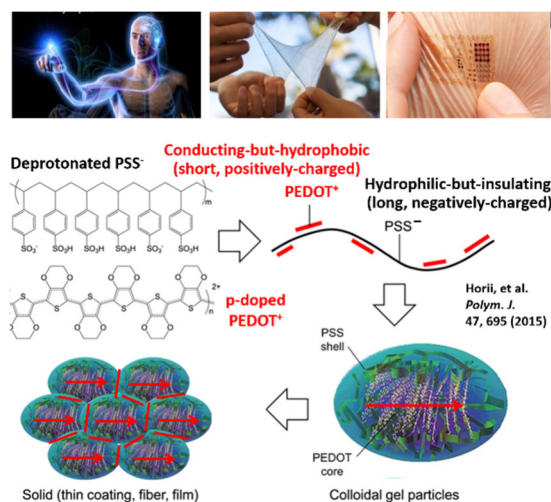

Figure 2. (Top) Prospective applications of PEDOT:PSS in organic bioelectronics and (bottom) schematic origins of low conductivities of pristine PEDOT:PSS films.

A remarkable (~5,000-fold) improvement in conductivity has been achieved by vigorously mixing PEDOT:PSS with an ionic liquid (IL) of 1-ethyl-3-methylimidazolium (EMIM$^+$) cation and tetracyanoborate (TCB$^-$) anion.[12,13] Various experiments indicate a mechanism where the IL ion pairs, EMIM$^+$:TCB$^-$, trigger ion exchanges with PEDOT$^+$:PSS$^-$ and help PEDOT$^+$ decouple from PSS$^-$ and grow into a large conducting domain decorated by TCB$^-$ anions (Fig. 3). Our free energy estimations using density functional theory (DFT) and molecular dynamics (MD) simulation[13-16] exhibit the central role played by the classic hard-soft-acid-base principles[17-20] in this mechanism. The deprotonated PSS$^-$ is a hydrophilic (hard) anion (base) that can form hydrogen (H) bonds with water, and the p-doped PEDOT$^+$ is a hydrophobic (soft) cation (acid) that has a single positive charge dispersed over at least three π-conjugated EDOT units.[21-24] Hence, the most favorable ion exchange with PEDOT$^+$:PSS$^-$ would be achieved by ILs of the most hydrophobic anion (such as TCB$^-$) and the most hydrophilic cation (which is definitely not EMIM$^+$).

We herein propose that a new IL, MIM$^+$:TCB$^-$ (Fig. 3), where EMIM$^+$ was replaced by protic (thus more hydrophilic) 3-methylimidazolium MIM$^+$, can improve further the conductivity of PEDOT:PSS, and confirm it experimentally and computationally. We demonstrate the generality of this cation effect and its higher significance when paired with less effective (hydrophobic) bis(trifluoromethane)sulfonamide anion TFSI$^-$. Since a significant increase in stretchability is also observed during this course on the same film treated with MIM:TCB, we investigate the molecular origin of this improved stretchability of IL-treated PEDOT:PSS films as well.[25,26]
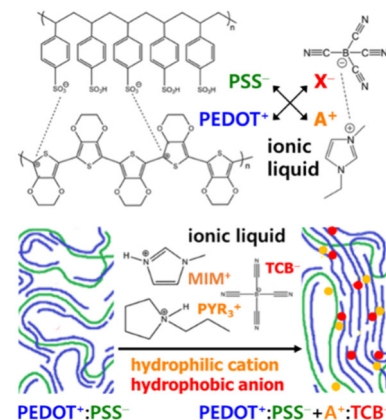

Figure 3. PEDOT-PSS separation and PEDOT domain growth induced by ion exchange with hard-cation-soft-anion ionic liquids.

2- Calculational details

DFT calculation (ion-exchange free energy). To predict the favorability of the ion exchange between PEDOT:PSS and MIM$^+$:TCB$^-$, the aqueous-phase ion-exchange free energy $\Delta G_{ex,aq}$ is estimated as ΔG_{aq} (PEDOT$^+$:TCB$^-$) + ΔG_{aq} (MIM$^+$:PSS$^-$) − ΔG_{aq} (PEDOT$^+$:PSS$^-$) − ΔG_{aq} (MIM$^+$:TCB$^-$). PEDOT and PSS are minimally modeled by an EDOT trimer with a unit positive charge (3EDOT$^+$) and a monomeric SS$^-$ (i.e., *p*-toluenesulfonate, PTS$^-$). The geometry of each ion pair is first optimized in the gas phase yielding the total energy E_g, then verified by a normal mode analysis which also yields the zero-point energy, ZPE, and the free energy correction at 298 K, $\Delta\Delta G_{0\to298K}$, and finally re-optimized in the Poisson–Boltzmann implicit solvation model to yield the hydration energy ΔG_{hyd}. The aqueous-phase free energy ΔG_{aq} is obtained as E_g + ZPE$_g$ + $\Delta\Delta G_{0\to298K,g}$ + ΔG_{hyd} and then combined to yield $\Delta\Delta G_{ex,aq}$. All the calculations are performed at the level of B3LYP/6-31++G** with *Jaguar* (Schrödinger).

MD simulation (morphology after IL mixing). Larger PEDOT:PSS models, i.e., 48 chains of doubly-charged six-unit oligomer 6EDOT^{2+} and either six chains of 16-unit fully-deprotonated oligomer 16SS^{16-} or 96 PTS$^-$ monomer units, are used. The PSS-to-PEDOT weight ratio (3:1) is comparable to 2.5:1 of the Clevios^{TM} PH1000 PEDOT:PSS solution.[13] They are mixed with 96 MIM:TCB pairs in a 12-nm periodic cubic box filled with ~54,000 SPC/E water molecules,[27] as done with EMIM:TCB in our previous study. Water molecules are randomly chosen from the final MD snapshot of the pristine PEDOT:PSS and replaced by 96 MIM:TCB pairs. The interactions of PEDOT:PSS and MIM:TCB are described by the OPLS-AA-based force field[28] supplemented with electrostatic-potential-fitted (ESP) atomic charges obtained from our DFT calculations. A particle-mesh Ewald summation implemented in GROMACS 5.1.4 analyzes the long-range electrostatic interactions, while the short-range interactions are truncated at 14 Å. After a short energy minimization, this model is subjected to a 60-ns NVT simulation with the modified Berendsen thermostat[29] at 293 K and then to simulated annealing runs (which linearly increase the temperature from 293 K to 363 K during 10-ns NPT run and decreases back to 293 K during 20-ns NPT run at 1 atm) in order to mimic IL mixing conducted in experiments, and finally to a 180-ns NPT simulation at 293 K and 1 atm with the Nose-Hoover thermostat and the Parrinello-Rahman barostat. A time step of 2 fs is used for the leap-frog integration. Cluster analyses using a friends-of-friends algorithm and a threshold distance of 3.5 Å retrieve the size and the composition of PEDOT clusters formed before and after mixing PEDOT:PSS with IL pairs.

MD simulation (film formation). Molecular models representing the spin-coated films of pristine and IL-treated PEDOT:PSS are built by first removing (virtually evaporating) all the water molecules from the final snapshots of pristine and IL-treated PEDOT:PSS aqueous solutions obtained above and then performing NPT simulating annealing up to 373 K with the Berendsen barostat.[30] Actual PEDOT:PSS films may contain non-negligible amounts of water,[7] affecting their elastic properties, but the water content would vary with experiment conditions and film history (e.g., pristine vs. IL-treated). We thus remove all the water molecule in both cases to identify the intrinsic IL effects (rather than the effect of IL-dependent water contents).

MD simulation (uniaxial stress-strain curve). The stress-strain curves of each film are derived from three uniaxial-tensile-loading simulations on the final snapshot. Each simulation stretches (increases the size of) the cell in a direction at a constant deformation rate (5×10^{-5} nm/ps) while compressing (decreasing the size of) the cell in the other directions under the external pressure (1 bar) with the anisotropic Berendsen barostat. The deformation continues until the film breaks. The pressure tensor P_i and the cell size L_i ($i = x, y, z$) are saved every 1 ps. They are converted to the stress σ ($= -P_i$) on the relative strain ε [$= (L_i - L_{0i}) / L_{0i}$], where L_{0i} is the cell size prior to the deformation ($t = 0$). The initial dependence $\sigma(\varepsilon)$ shows a linear regime up to 2% of deformation ε, and the elastic modulus E is defined as $\sigma = E\,\varepsilon$. The compressibility is set to zero along the deformation direction and to

4.5×10^{-10} Pa^{-1} to the planes perpendicular to the deformation direction

3- Results and discussion

The aqueous-phase ion-exchange free energy ($\Delta\Delta G_{ex,aq}$) is estimated as −23 (MIM:TCB), −18 (EMIM:TCB), −6 (MIM:TFSI), and −4 kJ/mol (EMIM:TFSI). More negative $\Delta\Delta G_{ex,aq}$ values indicate more favorable ion exchange (Fig. 4a-b). Indeed, the hydrophobic TCB$^-$ anion plays a key role in the ion exchange (−23 << −6 and −18 << −4), and the protic MIM$^+$ cation leads to a more favorable ion exchange than the aprotic EMIM$^+$ (−23 < −18 and −6 < −4), most likely due to its stronger H bonds with PSS$^-$, as shown by the short H-bond distance in the MIM:PSS ion pairs (2.85 Å for N---O; Fig. 4a).
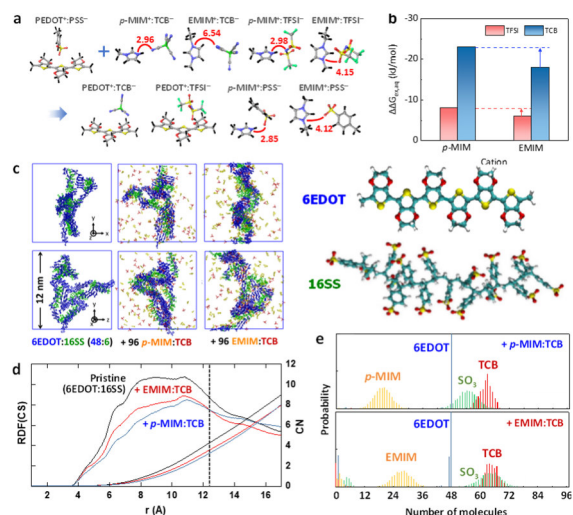

Figure 4. (a) DFT-optimized ion pairs before and after ion exchange between a minimal PEDOT:PSS model and four ILs. The distances (Å) between the H-bond donor (N of MIM/EMIM) and acceptor (N of TCB/TFSI and O of PSS) are shown in red [H (black), B (green), C (gray), N (blue), O (red), F (green), and S (yellow)]. (b) DFT ion-exchange free energies estimated in an implicit solvation model of water. (c) Final MD snapshots of pristine and IL-treated 6EDOT:16SS models [6EDOT$^+$ (blue), 16SS^{16-} (green), EMIM$^+$/MIM$^+$ (yellow), TCB$^-$ (red), and water (hidden)]. (d) RDF (solid) and CN (dotted) between the sulfonate S of 16SS and the backbone C of 6EDOT before (black) and after mixing with EMIM:TCB (red) or MIM:TCB (blue). (e) Friends-of-friends analyses (over the last 60-ns MD) of the size and composition of 6EDOT clusters formed after mixing with MIM:TCB (top) or EMIM:TCB (bottom) ILs.

Larger-scale MD simulations also confirm the favorable ion exchange induced by TCB-based ILs. The final snapshots taken after 270-ns MD simulations show no trace of self-agglomeration of ILs (Fig. 4c), suggesting their decent water solubility. Both ILs are either well-dispersed in the water phase or deposited on the surface of PEDOT or PSS. The IL-induced PEDOT-PSS separation and PEDOT assembly are not visible in these snapshots, but we clearly see it in the radial distribution function of the sulfonate S atoms of 16SS around the backbone C atoms of 6EDOT, RDF(C-S), averaged over the last 60 ns of the simulation (Fig. 4d), which is reduced after mixing with both ILs. Indeed, at short C-S distances (< 12 Å), the RDF reduction is more significant after mixing with MIM:TCB than with EMIM:TCB, implying more favorable ion exchange with MIM:TCB, as predicted by DFT. Interestingly, at long C-S distances (> 12 Å), the trend reverses so that RDF(C-S) is higher with MIM:TCB than with EMIM:TCB and their integrations, i.e., coordination numbers (CN), catch up each other (Fig. 4d). Our speculation is that the PSS chains, which are dissociated from PEDOT and pushed out of the large π-stacked PEDOT domains, still remain near the surface of these PEDOT domains by secondary bridges, PEDOT:TCB---MIM:PSS, which are favorably mediated by protic and planar MIM, i.e., by its H bonds with PSS and TCB as well as its π-stacking with PEDOT. Such PSS chains holding multiple PEDOT domains together can enhance the elastic property of the film, as confirmed experimentally (Fig. 5, ii and v). Since such TCB---MIM:PSS bridges stay on outer surfaces of PEDOT domains, the film may lose them by an excess amount of water or acetonitrile, losing the elastic improvements as well, as confirmed in the experiments (Fig. 5, left, iii-iv).
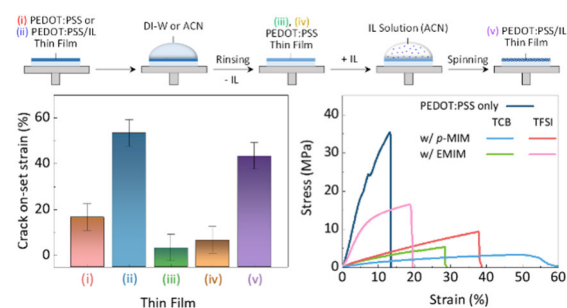

Figure 5. (Top) PEDOT:PSS thin films and (bottom) their crack onset strains ε_c (left) and stress-strain curves (right), which show the importance of protic IL, MIM/TCB.

From the size and composition of the 6EDOT clusters formed after IL mixing (Fig. 4e), we see

that a higher degree of PEDOT-PSS separation is induced by MIM:TCB than by EMIM:TCB. With MIM:TCB, the whole 48 6EDOT units form a single stable cluster with ~55 (out of 96) sulfonate (SO_3^-) groups of 16SS attached to it, while the 48-unit 6EDOT cluster is less stable (occasionally breaking into two fragments) and has more (~65) SO_3^- groups attached to it after EMIM:TCB treatment. This is consistent with the trend shown in the short-range RDF(C-S). The two graphs in Fig. 4e also show that the 6EDOT cluster contains fewer IL components after being treated with MIM:TCB (~60 TCB^- anions, blue bars; ~18 MIM^+ cations, red bars) than after being treated with EMIM:TCB (~65 TCB^- anions and ~30 $EMIM^+$ cations). It can be that planar and hydrophobic $EMIM^+$ tends to bind (or even intercalate) to the hydrophobic PEDOT domain, which may adversely interfere with the separation of $EMIM^+{:}SO_3^-$ pairs from the PEDOT domain as well as the π-stacking (and/or electron transfer through the π-stacking) of PEDOT units in that domain, and this appears to be partially avoided using hydrophilic MIM^+ cations. However, a significant amount of planar MIM^+ cations still remain around the PEDOT:TCB domains (via H bonds with TCB and π-stacking with PEDOT) while bonded to a significant (but not excessive) amount of PSS (via strong H bonds). Such MIM-mediated secondary bridges (PEDOT:TCB---MIM:PSS) would enhance the stretchability of the PEDOT films, as confirmed by our preliminary uniaxial
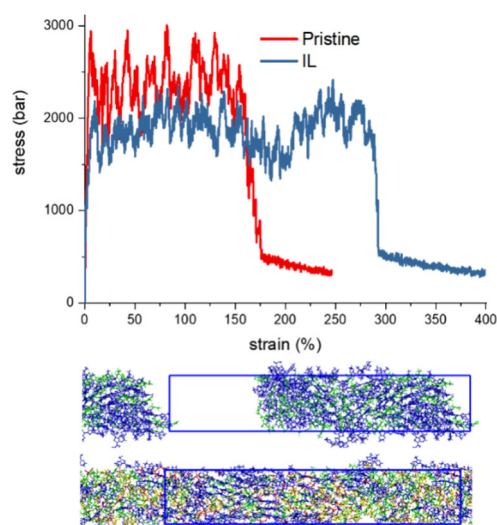
stress-strain-curve simulations (Fig. 7).

Figure 7. Preliminary stress-strain curves and snapshots of pristine and IL-treated PEDOT:PSS films at 200% strain.

4- Conclusion

Combining our small-scale DFT calculation and large-scale MD simulation as well as various experiments in collaboration, we predicted, confirmed, and understood the improvement of both electrical (conductivity) and mechanical (stretchability) properties of PEDOT:PSS films induced by hard-cation-soft-anion ILs such as MIM:TCB composed of protic MIM^+ cations and hydrophobic TCB^- anions.

5- Perspectives of future collaborations with the host laboratory

While PEDOT:PSS is a polyelectrolyte with a tremendous industrial importance, DNA/RNA are polyelectrolytes with tremendous biological importance. Just like PEDOT:PSS composed of stiff cations PEDOT and flexible anions PSS, DNA is one of the longest and stiffest anionic molecules in nature, which is condensed in a tiny space of cell nuclei by various cationic peptides. DNA is condensed even further during cell division or in sperm cells by a special cationic peptide, protamine. Understanding the principles underlying such fascinating and dynamic processes between DNA/RNA and protamine would bring us one step closer not only to the origin of life but also to applications in various fields such as medicine, materials, and energy, but it is still difficult to observe such processes at the molecular level by real experiments. Hence, our current project on IL-induced PEDOT:PSS phase change, which can be considered as a type of controlled liquid-liquid phase separation, has a broad relevance to protein-controlled DNA packaging in vivo and in vitro as well as controlled packaging and de-packaging of recent antiviral and anticancer mRNA vaccines platforms. Therefore, as an immediate extension of our current project on PEDOT:PSS, we continue our molecular-level simulation on reversible condensation between DNA/RNA and protamine (Fig. 7). This will eventually lead us to the mechanism of gene transfer and protection in the cell nuclei or in viruses and to the development of anticancer-antiviral mRNA vaccines.[31-33]
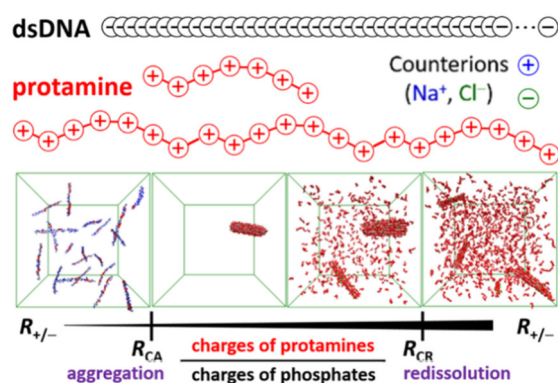
Figure 7. MD simulation on generic coarse-grained models capturing the correct average linear charge densities on DNA and protamine for correct evaluation of their long-range electrostatic interactions.

On the other hand, PEDOT:PSS is a conducting polymer, which will eventually become low-cost, light-weight, and flexible alternatives (*soft electronics*) to current silicon-based electronic-device materials. Essentially an infinite number of chemical design is possible for conducing polymers with promising properties. Therefore, our current project is extended to a molecular-level understanding and rational design of electronic, optical, and mechanical properties of various conducting polymers as soft electronics components. As an example, we design a red-selective polymer which can strongly absorb only the skin-penetrating visible light, i.e., the red light of wavelengths 625~800 nm (Fig. 8). Such a polymer will help realizing wireless (i.e., non-invasive) power supply to a subdermal bioelectronic implant (e.g., pacemaker on heart or neuromodulator on brain) by shedding the red light toward the red-light-absorbing organic photovoltaic thin film deposited on it. Such a polymer can also be used as a conformable RGB-color-selective photodiode component, which will help realizing retinal prosthesis and vision restoration.[34,35]
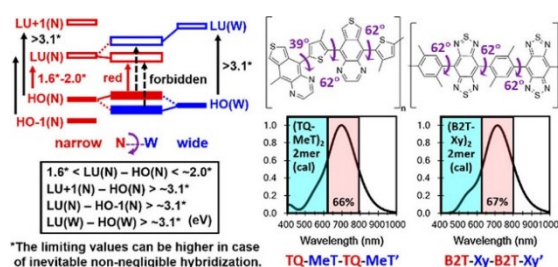

Figure 8. (Left) Detailed design principles (in eV) and (b) newly-designed examples of narrow-wide red-selective polymers.[34,35]

6- Articles published in the framework of the fellowship

(1) M. Kim, S. Y. Lee, J. Kim, C. Choi, Y. Lansac, H. Ahn, S. Park, Y. H. Jang,* S. H. Lee,* B. H. Lee,* Protic Ionic Liquids for Intrinsically Stretchable Conductive Polymer, *ACS Appl. Mater. Interfaces*, 15, 3202-3213 (2023)

(2) Y. H. Jang,* E. Raspaud, Y. Lansac,* DNA-Protamine Condensates under Low Salt Conditions: Molecular Dynamics Simulation with a Simple Coarse-Grained Model Focusing on Electrostatic Interactions, *Nanoscale Adv.* 5, 4798-4808 (2023)

(3) W. Jeon, C. Choi, J. Cheon, J. Lee, Y. Lansac, Y. H. Jang,* Narrow-Wide Copolymers Designed for Red-Selective Absorption by Time-Dependent Density Functional Theory Calculations, *J. Phys. Chem. C* 127, 31, 15290-15299 (2023)

(4) K. B. Chhetri, Y. H. Jang,* Y. Lansac,* P. K. Maiti,* Effect of Phosphorylation of Protamine-Like Cationic Peptide on the Binding Affinity to DNA, *Biophy. J.* 121, 4830-4839 (2022)

(5) C. Choi, W. Jeon, Y. Lansac,* Y. H. Jang,* Narrow-Wide Copolymer for Strong Red-Color-Selective Absorption, *J. Phys. Chem. C* 126, 12230-12237

(2022) – published between the application and the program

(6) C. Choi, A. de Izarra, I. Han, W. Jeon, Y. Lansac,* Y. H. Jang,* Hard-Cation-Soft-Anion Ionic Liquids for PEDOT:PSS Treatment. *J. Phys. Chem. B* 2022, 126, 1615-1624. – published between the application and the program

(7) K. B. Chhetri, Y. H. Jang,* Y. Lansac,* P. K. Maiti,* DNA Groove Preference Shift upon Phosphorylation of a Protamine-Like Cationic Peptide, *Phys. Chem. Chem. Phys.* (under revision)

(8) A. Ricard, F. Restagno, Y. H. Jang, Y. Lansac, E. Raspaud,* Corrosion-Driven Droplet Wetting on Iron Nanolayers, *Sci. Rep.* (under review)

(9) C. Choi, Y. Lansac, Y. H. Jang,* Proceedings of APCE-CECE-ITP-IUPAC 2022. 45. Morphology Control of PEDOT:PSS Polyelectrolyte by Hard-Cation-Soft-Anion Ionic Liquids: Microscopic Observation by Molecular Dynamics Simulation, *Separations*, 10, 109 (2023) – Conference Proceeding

(10) Y. Lansac,* Y. H. Jang, A. Mukherjee, J. Degrouard, Proceedings of APCE-CECE-ITP-IUPAC 2022. 46. Protamine-Controlled Reversible DNA Packaging: A Molecular Glue, *Separations*, 10, 109 (2023) – Conference Proceeding

7- Acknowledgements

8- References

(1) Takano, T.; Masunaga, H.; Fujiwara, A.; Okuzaki, H.; Sasaki, T. PEDOT Nanocrystal in Highly Conductive PEDOT:PSS Polymer Films. *Macromolecules* 2012, 45, 3859-3865.

(2) Honma, Y.; Itoh, K.; Masunaga, H.; Fujiwara, A.; Nishizaki, T.; Iguchi, S.; Sasaki, T. Mesoscopic 2D Charge Transport in Commonplace PEDOT:PSS Films. *Adv. Electron. Mater.* 2018, 4, 1700490.

(3) Kim, N.; Kee, S.; Lee, S. H.; Lee, B. H.; Kahng, Y. H.; Jo, Y.-R.; Kim, B.-J.; Lee, K. Highly Conductive PEDOT:PSS Nanofibrils Induced by Solution-Processed Crystallization. *Adv. Mater.* 2014, 26, 2268-2272.

(4) Palumbiny, C. M.; Liu, F.; Russell, T. P.; Hexemer, A.; Wang, C.; Müller-Buschbaum, P. The Crystallization of PEDOT:PSS Polymeric Electrodes Probed In Situ during Printing. *Adv. Mater.* 2015, 27, 3391-3397.

(5) Fan, Z.; Du, D.; Yu, Z.; Li, P.; Xia, Y.; Ouyang, J. Significant Enhancement in the Thermoelectric Properties of PEDOT:PSS Films through a Treatment with Organic Solutions of Inorganic Salts. *ACS Appl. Mater. Interfaces* 2016, 8, 23204-23211.

(6) Modarresi, M.; Mehandzhiyski, A.; Fahlman, M.; Tybrandt, K.; Zozoulenko, I. Microscopic Understanding of the Granular Structure and the Swelling of PEDOT:PSS. *Macromolecules* 2020, 53, 6267-6278.

(7) Modarresi, M.; Franco-Gonzalez, J. F.; Zozoulenko, I. Computational Microscopy Study of the Granular Structure and pH Dependence of PEDOT:PSS. *Phys. Chem. Chem. Phys.* 2019, 21, 6699-6711.

(8) Li, Y.; Tanigawa, R.; Okuzaki, H. Soft and Flexible PEDOT/PSS Films for Applications to Soft Actuators. *Smart Mater. Struct.* 2014, 23, 074010.

(9) Lang, U.; Müller, E.; Naujoks, N.; Dual, J. Microscopical Investigations of PEDOT:PSS Thin Films. *Adv. Func. Mater.* 2009, 19, 1215-1220.

(10) Dimitriev, O. P.; Piryatinski, Y. P.; Pud, A. A. Evidence of the Controlled Interaction between PEDOT and PSS in the PEDOT:PSS Complex via Concentration Changes of the Complex Solution. *J. Phys. Chem. B* 2011, 115, 1357-1362.

(11)   Yan, H.; Arima, S.; Mori, Y.; Kagata, T.; Sato, H.; Okuzaki, H. Poly(3,4-Ethylenedioxythiophene)/Poly(4-Styrenesulfonate): Correlation between Colloidal Particles and Thin Films. *Thin Solid Films* **2009**, *517*, 3299-3303.

(12)   Badre, C.; Marquant, L.; Alsayed, A. M.; Hough, L. A. Highly Conductive Poly(3,4-ethylenedioxythiophene):Poly(styrenesulfonate) Films Using 1-Ethyl-3-methylimidazolium Tetracyanoborate Ionic Liquid. *Adv. Func. Mater.* **2012**, *22*, 2723-2727.

(13)   Kee, S.; Kim, N.; Kim, B. S.; Park, S.; Jang, Y. H.; Lee, S. H.; Kim, J.; Kim, J.; Kwon, S.; Lee, K. Controlling Molecular Ordering in Aqueous Conducting Polymers Using Ionic Liquids. *Adv. Mater.* **2016**, *28*, 8625-8631.

(14)   de Izarra, A.; Park, S.; Lee, J.; Lansac, Y.; Jang, Y. H. Ionic Liquid Designed for PEDOT:PSS Conductivity Enhancement. *J. Am. Chem. Soc.* **2018**, *140*, 5375-5384.

(15)   de Izarra, A.; Choi, C.; Jang, Y. H.; Lansac, Y. Ionic Liquid for PEDOT:PSS Treatment. Ion Binding Free Energy in Water Revealing the Importance of Anion Hydrophobicity. *J. Phys. Chem. B* **2021**, *125*, 1916-1923.

(16)   de Izarra, A.; Choi, C.; Jang, Y. H.; Lansac, Y. Molecular Dynamics of PEDOT:PSS Treated with Ionic Liquids. Origin of Anion Dependence Leading to Cation Design Principles. *J. Phys. Chem. B* **2021**, *125*, 8601-8611.

(17)   Pearson, R. G. Hard and Soft Acids and Bases. *J. Am. Chem. Soc.* **1963**, *85*, 3533-3539.

(18)   Klopman, G. Chemical Reactivity and the Concept of Charge- and Frontier-Controlled Reactions. *J. Am. Chem. Soc.* **1968**, *90*, 223-234.

(19)   Pearson, R. G. Hard and Soft Acids and Bases, HSAB, Part I. Fundamental principles. *J. Chem. Educ.* **1968**, *45*, 581-587.

(20)   Pearson, R. G. Hard and Soft Acids and Bases, HSAB, Part II. Underlying Theories. *J. Chem. Educ.* **1968**, *45*, 643-648.

(21)   Zotti, G.; Zecchin, S.; Schiavon, G.; Louwet, F.; Groenendaal, L.; Crispin, X.; Osikowicz, W.; Salaneck, W.; Fahlman, M. Electrochemical and XPS Studies toward the Role of Monomeric and Polymeric Sulfonate Counterions in the Synthesis, Composition, and Properties of Poly(3,4-ethylenedioxythiophene). *Macromolecules* **2003**, *36*, 3337-3344.

(22)   Kahol, P. K.; Ho, J. C.; Chen, Y. Y.; Wang, C. R.; Neeleshwar, S.; Tsai, C. B.; Wessling, B. On Metallic Characteristics in Some Conducting Polymers. *Synth. Met.* **2005**, *151*, 65-72.

(23)   Kirchmeyer, S.; Reuter, K. Scientific Importance, Properties and Growing Applications of Poly(3,4-ethylenedioxythiophene). *J. Mater. Chem.* **2005**, *15*, 2077-2088.

(24)   Kim, D.; Zozoulenko, I. Why Is Pristine PEDOT Oxidized to 33%? A Density Functional Theory Study of Oxidative Polymerization Mechanism. *J. Phys. Chem. B* **2019**, *123*, 5160-5167.

(25)   Choi, C.; de Izarra, A.; Han, I.; Jeon, W.; Lansac, Y.; Jang, Y. H. Hard-Cation-Soft-Anion Ionic Liquids for PEDOT:PSS Treatment. *J. Phys. Chem. B* **2022**, *126*, 1615-1624.

(26)   Kim, M.; Lee, S. Y.; Kim, J.; Choi, C.; Lansac, Y.; Ahn, H.; Park, S.; Jang, Y. H.; Lee, S. H.; Lee, B. H. Protic Ionic Liquids for Intrinsically Stretchable Conductive Polymers. *ACS Appl. Mater. Interfaces* **2023**, *15*, 3202-3213.

(27)   Berendsen, H. J. C.; Grigera, J. R.; Straatsma, T. P. The Missing Term in Effective Pair Potentials. *J. Phys. Chem.* **1987**, *91*, 6269-6271.

(28)   Franco-Gonzalez, J. F.; Zozoulenko, I. V. Molecular Dynamics Study of Morphology of Doped PEDOT: From Solution to Dry Phase. *J. Phys. Chem. B* **2017**, *121*, 4299-4307.

(29) Bussi, G.; Donadio, D.; Parrinello, M. Canonical sampling through velocity rescaling. *J. Chem. Phys.* **2007**, *126*, 014101.

(30) Berendsen, H. J. C.; Postma, J. P. M.; van Gunsteren, W. F.; DiNola, A.; Haak, J. R. Molecular Dynamics with Coupling to an External Bath. *J. Chem. Phys.* **1984**, *81*, 3684-3690.

(31) Mukherjee, A.; de Izarra, A.; Degrouard, J.; Olive, E.; Maiti, P. K.; Jang, Y. H.; Lansac, Y. Protamine-Controlled Reversible DNA Packaging: A Molecular Glue. *ACS Nano* **2021**, *15*, 13094-13104.

(32) Mukherjee, A.; Saurabh, S.; Olive, E.; Jang, Y. H.; Lansac, Y. Protamine Binding Site on DNA: Molecular Dynamics Simulations and Free Energy Calculations with Full Atomistic Details. *J. Phys. Chem. B* **2021**, *125*, 3032-3044.

(33) Jang, Y. H.; Raspaud, E.; Lansac, Y. DNA-Protamine Condensates under Low Salt Conditions: Molecular Dynamics Simulation with a Simple Coarse-Grained Model Focusing on Electrostatic Interactions. *Nanoscale Adv.* **2023**, *5*, 4798-4808.

(34) Choi, C.; Jeon, W.; Lansac, Y.; Jang, Y. H. Narrow-Wide Copolymer for Strong Red-Color-Selective Absorption. *J. Phys. Chem. C* **2022**, *126*, 12230-12237.

(35) Jeon, W.; Choi, C.; Cheon, J.; Lee, J.; Lansac, Y.; Jang, Y. H. Narrow–Wide Copolymers Designed for Red-Selective Absorption by Time-Dependent Density Functional Theory Calculations. *J. Phys. Chem. C* **2023**, *127*, 15290-15299.